

Simulated photoelectron intensities at the aqueous solution–air interface for flat and cylindrical (microjet) geometries

Received 00th January 20xx,
Accepted 00th January 20xx

Giorgia Olivieri,^a Krista M. Parry,^b Cedric J. Powell,^c Douglas J. Tobias^b and Matthew A. Brown^{a*}

DOI: 10.1039/x0xx00000x

www.rsc.org/

Ion spatial distributions at the aqueous-air/vacuum interface are accessible by energy-dependent X-ray photoelectron spectroscopy (XPS). Here we quantify the difference between a flat surface and a cylindrical shaped microjet on the energy-dependent information depth of the XPS experiment and on the simulated photoelectron intensities using solutions of pure water and of 1 mol/L NaI as examples.

Photoelectron spectroscopy from liquid solutions dates to the pioneering laboratory-based work of Hans and Kai Siegbahn in the early nineteen-seventies.¹ The majority of current work in this field is now performed using synchrotron light sources^{2–4} that have the advantage of significantly higher brilliance than a laboratory anode tube and the ability to vary the X-ray energy. The latter permits depth-resolved experiments by exploiting the dependence of the information depth (ID) with kinetic energy of the photoelectron in solution⁵ and has been used extensively to interrogate the spatial distributions of electrolyte ions at aqueous-air/vacuum interfaces.^{6–13} These interfaces are routinely generated by deliquescing a salt crystal in an ambient pressure (several hundred Pa) of water vapour,^{6, 7, 11, 12} or by passing an electrolyte solution through a small capillary to create a free-flowing filament (a liquid microjet) in a vacuum of about 10^{-2} Pa.^{9, 10, 13} While it is generally assumed that these two experimental configurations give similar results, the liquid interfaces they create have two very different geometries: (assumed) flat in the case of a deliquesced sample (aqueous-air interface) and cylindrical when using the microjet (aqueous-vacuum interface). In this *Communication* we explore the effects of these different geometries on the energy-dependent ID of the XPS experiment

and on the depth-resolved simulated photoelectron intensities of pure water and of 1 mol/L NaI (with a focus on the I^-/Na^+ ratio).

The ID of a particular XPS experiment is determined in large part by the inelastic mean free path (IMFP) and the emission angle (α) of the photoelectrons with respect to the surface normal.^{14,15} ID calculations have only been made for photoelectron spectroscopy experiments that employ unpolarised X-rays;^{14,15} however, ion spatial distributions of aqueous electrolyte solutions have, to-date, only been measured using linearly polarized X-rays.^{6–13} Using the Simulation of Electron Spectra for Surface Analysis (SESSA) database developed by Werner *et al.*,^{16,17} we calculate the ID of an XPS experiment that employs linearly polarized light at a semi-infinite solution as a function of the percentage of the detected signal, P , when $\alpha = 0^\circ$. Results for a solution of pure water are shown in Fig. 1a for photoelectron kinetic energies of 65 eV and 1500 eV (see ESI for details). The corresponding IDs for photoelectron kinetic energies between 65 eV and 1500 eV when $\alpha = 0^\circ$ are shown in Fig. 1b (Table ESI-1, results for 1 mol/L NaI are available in the ESI) for our choice of $P = 95\%$. This energy range corresponds roughly to that typically available at soft X-ray synchrotron beamlines. For an experiment performed using a cylindrical microjet the average emission angle is not immediately clear and needs to be first calculated before the correct ID can be properly determined.

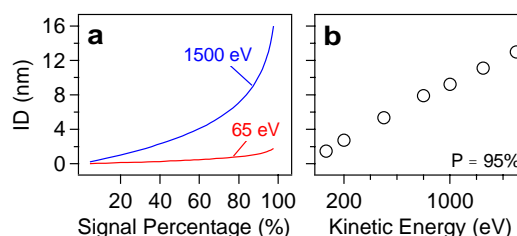


Fig. 1 (a) Information depth (ID) at 65 eV and 1500 eV of a semi-infinite solution of pure water as a function of the percentage of the detected signal when using linearly polarized light and $\alpha = 0^\circ$. (b) IDs of liquid water for $P = 95\%$ as a function of photoelectron kinetic energy when $\alpha = 0^\circ$.

^a Laboratory for Surface Science and Technology, Department of Materials, ETH Zürich, Switzerland. E-mail: matthew.brown@mat.ethz.ch

^b Department of Chemistry, University of California, Irvine, California, USA.

^c Materials Measurement Science Division, National Institute of Standards and Technology, Gaithersburg, Maryland, USA.

Electronic Supplementary Information (ESI) available: Table ESI-1, Figs. ESI-1, ESI-2, ESI-3 and ESI-4, and details of the simulation of electron spectra for surface analysis (SESSA) and molecular dynamics (MD) simulations. See DOI: 10.1039/x0xx00000x

To model an XPS experiment that employs a liquid microjet, the cylindrical geometry is reconstructed by a series of planes that run tangent to the outer surface of the microjet (Fig. 2a). Only planes from quadrant 1 (Q1, with plane tilt angles $\theta = 0^\circ$ to 90°)

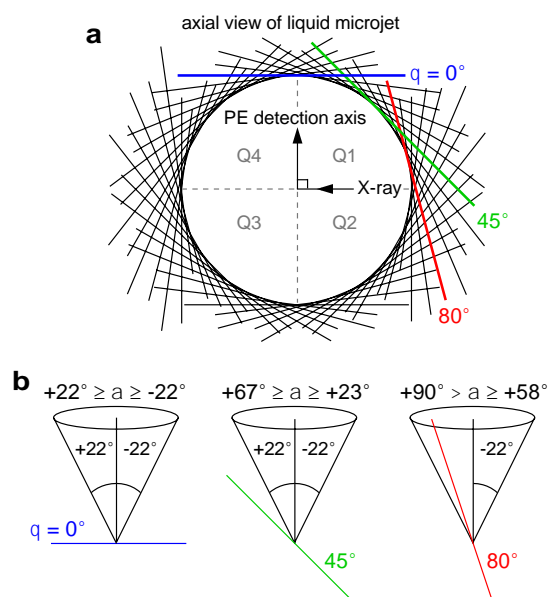


Fig. 2 (a) Model of a cylindrical microjet used for photoelectron spectroscopy measurements of liquid solutions. The direction of liquid flow, incident X-ray and photoelectron (PE) detection axis are orthogonal. The cylindrical shape of the microjet is modelled using a series of planes that reconstruct the interfaces' curvature. The cylinder is divided into four quadrants (Q1–Q4) and only photoelectrons from Q1 reach the detector. (b) The photoelectron emission angles (α) that contribute to intensity depend on the plane tilt angle (in colour for $\theta = 0^\circ$, 45° and 80°) and the analyser polar acceptance angle (shown here for $\phi = \pm 22^\circ$). For planes with high tilt angles, the angular acceptance of the analyser is cut by the surface (e.g., $\theta = 80^\circ$).

contribute to the measured intensity¹⁸; photoelectrons from Q2 are blocked by Q1 (due to the short IMFPs of the detected photoelectrons), whereas Q3 and Q4 are shadowed by Q1 and Q2 from the incoming X-ray (due to the finite penetration depth of soft X-rays). The photoelectron emission angles (α) from each plane that contribute intensity in an experiment are a function of the polar acceptance angle of the analyser, ϕ . Figure 2b shows the accepted emission angles for $\theta = 0^\circ$, 45° and 80° when the analyser polar acceptance angle is $\phi = \pm 22^\circ$ (common to modern differentially-pumped hemispherical analysers¹⁹). For planes with tilt angles of $\theta = 0^\circ$ and 45° , the full angular acceptance of the analyser is realised, whereas for planes with higher tilt angles the angular acceptance of the analyser is cut by the surface (see Fig. 2b, $\theta = 80^\circ$) and the intensity reaching the analyser is decreased accordingly.

Using SESSA we simulate the O 1s photoelectron intensity from a semi-infinite solution of pure water as a function of plane tilt angle for photoelectron kinetic energies between 65 eV and 1500 eV (see ESI for details). The O 1s intensities predicted by SESSA are scaled by a geometric weighting factor, g , that accounts for the projection of each plane onto an axis perpendicular to the photoelectron detection axis.²⁰ In our

model, this correction is $g = \cos \theta$. Figure 3a shows the results for a photoelectron kinetic energy of 65 eV when the analyser polar acceptance angle is $\phi = \pm 1^\circ$ (red circles). The decrease in O 1s intensity as the plane tilt angle is increased is well reproduced by the modified Chandrasekhar function, H (Fig. 3a):²²

$$H(\mu, \omega) = \frac{1 + \mu\sqrt{3}}{1 + \mu\sqrt{3(1-\omega)}} g \quad (1)$$

where $\mu = \cos \alpha$ and ω is the single-scattering albedo defined²² as the ratio of the IMFP to the sum of the IMFP and the transport mean free path ($\omega = 0.418$ at 65 eV for a solution of pure water).⁵

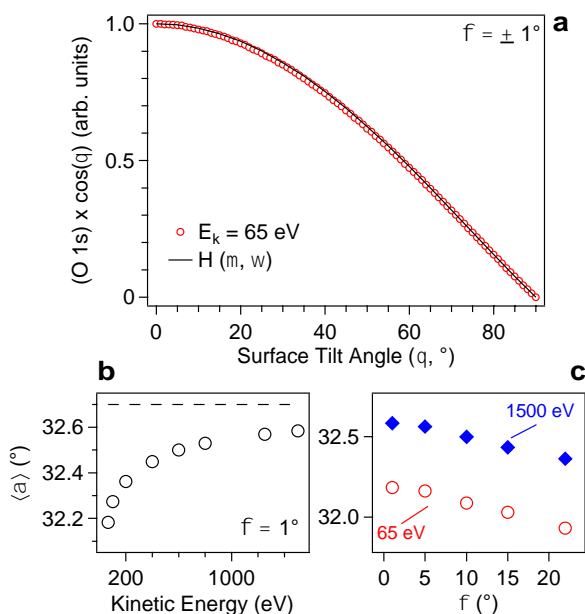


Fig. 3 (a) Simulated O 1s photoelectron intensities for a semi-infinite solution of pure water as a function of surface tilt angle (θ) at a kinetic energy (E_k) of 65 eV (open symbols). The polar acceptance angle of the analyser is $\phi = \pm 1^\circ$. The solid line is the modified Chandrasekhar function (Eq. 1) with $\omega = 0.418$. (b) Average photoelectron emission angle ($\langle \alpha \rangle$) from a cylindrical microjet as a function of kinetic energy when $\phi = \pm 1^\circ$. (c) Average photoelectron emission angle ($\langle \alpha \rangle$) from a cylindrical microjet as a function of polar acceptance angle of the analyser. Results are shown for kinetic energies of 65 eV (open red symbols) and 1500 eV (closed blue symbols).

The average emission angle ($\langle \alpha \rangle$) for an XPS experiment performed with a cylindrical microjet is calculated from the weighted average of the corresponding intensities in Fig. 3a:

$$\langle \alpha \rangle = \lim_{n \rightarrow \infty} \frac{\sum_{i=1}^n (I_i \cos \theta_i) \theta_i}{\sum_{i=1}^n I_i \cos \theta_i}, \quad (2)$$

where $I_i \cos \theta_i$ is the weighted intensity reaching the detector from the i -th plane, θ_i (see Fig. ESI–2). Results for photoelectron kinetic energies between 65 eV and 1500 eV are shown in Fig. 3b. The average emission angle from a homogeneous cylindrical microjet of pure water is $\langle \alpha \rangle = 32.2^\circ$ at 65 eV, increasing slightly to $\langle \alpha \rangle = 32.6^\circ$ by 1500 eV. The latter approaches the upper limit of 32.7° (dashed-line in Fig. 3b) for a cylindrical geometry derived from the straight-line approximation²² where all elastic-scattering events are neglected. The polar acceptance angle (ϕ) of the analyser has

no significant effect on the results up to $\phi = \pm 22^\circ$ (Fig 3c).²³ In addition, we find these results are independent of chemical composition: A homogeneous solution of 1 mol/L NaI yields virtually identical results to that of pure water (Fig. ESI-2).

The average emission angles in Fig. 3b are subsequently used to calculate the ID of an XPS experiment with cylindrical geometry. Continuing to use pure water as an example, we find that the ID at 65 eV decreases from 1.47 nm for a flat interface ($\alpha = 0^\circ$) to 1.36 nm in the cylindrical geometry ($\langle\alpha\rangle = 32.2^\circ$), and from 13.00 nm to 11.53 nm ($\langle\alpha\rangle = 32.6^\circ$) at 1500 eV. Overall, the effect of the cylindrical geometry of the liquid microjet is to increase the surface sensitivity of the experiment when compared to that of a flat surface.

Transitioning from a semi-infinite system to the interface region of a real solution adds complexity, as the solution is no longer homogeneous with depth. In electrolyte solutions, atomic populations in the vicinity of the aqueous-air/vacuum interface are typically depicted as density profiles determined by molecular dynamics (MD) simulations.²⁴ The profiles derived from MD simulations of an aqueous solution of 1 mol/L NaI are shown in Fig. 4, where zero depth is the position of the instantaneous interface (see ESI for details).²⁵ An enhancement of the ion population in the vicinity of the interface relative to the bulk is observed for both ions, while the water profile (oxygen density) shows clear layering near the interface. A detailed description of the driving forces behind these non-monotonic atom-density profiles is beyond the scope of the current work, but is discussed in detail in a recent review.²⁴ Here, using the MD density profiles of Fig. 4 and SESSA we predict the XPS intensities (I/Na^+ ratio) as a function of kinetic energy for a flat interface and for a cylindrical microjet. We note, however, that SESSA considers only atomic properties and each layer of the solution is modelled as being amorphous in structure. As such, any anisotropy that may be present in solution cannot be accounted for with SESSA.

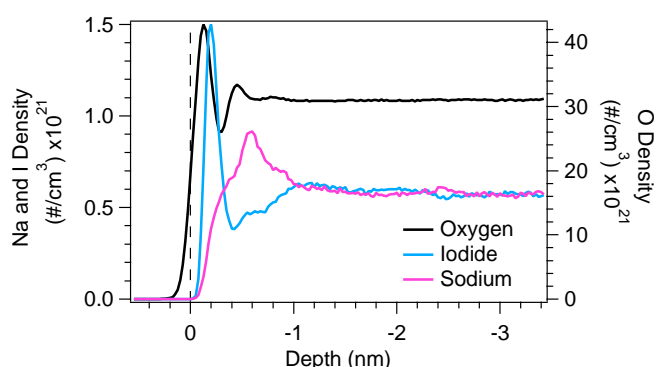


Fig. 4 Atomic density profiles determined from molecular dynamics (MD) simulations of 1 mol/L NaI. Black, oxygen (O) density (right axis); pink, sodium (Na) density (left axis); blue, (I) iodide density (left axis). The instantaneous interface is at $x = 0$ nm and marked by a dashed line. Negative x -values indicate depth into the solution.

The average emission angles $\langle\alpha\rangle$ for the MD-derived density profiles of 1 mol/L NaI in the cylindrical geometry of a microjet are shown in Fig. 5a for kinetic energies between 65 eV and 1500 eV. In contrast with the equivalent homogeneous

solution (Fig. ESI-3) we find a non-negligible kinetic-energy dependence of the average emission angle that ranges from $\langle\alpha\rangle = 27.5^\circ$ at 65 eV to $\langle\alpha\rangle = 32.5^\circ$ at 1500 eV. The average emission angles of iodide (4d) and sodium (2p) deviate from one another because of their unique density profiles, behaviour that is not seen in homogeneous systems where each component has the same energy-dependence.

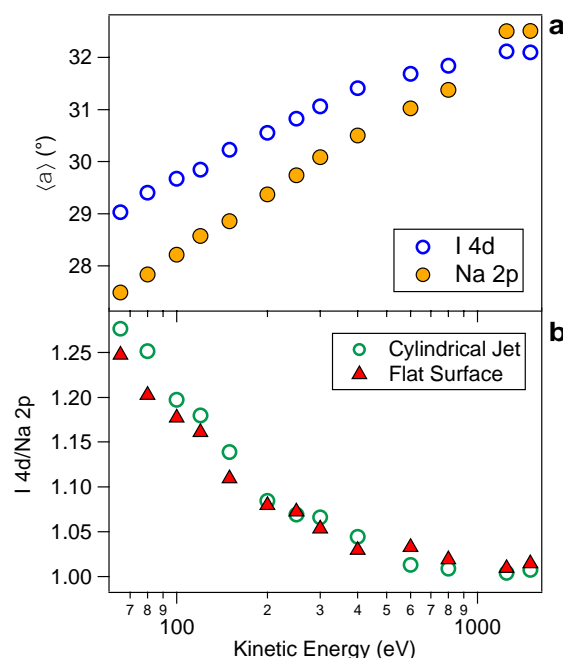


Fig. 5 (a) Average photoelectron emission angle ($\langle\alpha\rangle$) for a cylindrical microjet of 1 mol/L NaI (using the MD derived ion profiles of Fig. 4) as a function of kinetic energy. Results for the I 4d (open markers) and Na 2p (closed markers) orbitals are shown. The polar analyser acceptance angle is $\phi = \pm 1^\circ$. (b) SESSA calculated iodide-to-sodium ratio (I 4d/Na 2p) as a function of kinetic energy for a flat surface where $\alpha = 0^\circ$ (closed markers) and for a cylindrical microjet where $\alpha = \langle\alpha\rangle$.

The I 4d/Na 2p intensity ratio for a cylindrical microjet of 1 mol/L NaI is calculated using SESSA as a function of the photoelectron kinetic energy at the average emission angle (open green markers of Fig. 5b).²⁶ In agreement with the generally accepted picture of aqueous iodide electrolyte solutions,⁶ we find preferential enhancement of iodide relative to sodium at lower kinetic energies (the I 4d/Na 2p ratio is 1.28 at 65 eV). As the kinetic energy is increased, the intensity ratio decreases, eventually reaching a stoichiometric value at ≈ 600 eV. At this energy the ID has increased to a value (5.71 nm, see Table ESI-1) where the corresponding experiment could no longer be considered interface sensitive (an XPS experiment at this energy would be largely considered as a measure of bulk stoichiometry).

The results for the cylindrical geometry of a microjet are compared with those predicted for the same MD atom density profiles at a flat interface, $\alpha = 0^\circ$ (closed red symbols, Fig. 5b). The slight increase in surface sensitivity of the XPS experiment with the cylindrical geometry of the microjet has a negligible effect on the I 4d/Na 2p ion ratio. The predicted ion ratios differ by at most 4% at 65 eV and are indistinguishable at kinetic energies above 200 eV. Given the limitations of

reproducibility with XPS measurements at liquid interfaces, we predict these subtle differences in the intensity ratio could not be determined by experiment. Effectively, there is no difference between a flat interface and that of a cylindrical microjet from the perspective of an XPS experiment.

Conclusions

Using SESSA and atom-density profiles from MD simulations we determined the average emission angle for an XPS experiment performed from a cylindrical microjet. While the average emission angles are significant ($\approx 30^\circ$), the effect on the simulated ion intensity ratio (I 4d/Na 2p) for an aqueous solution of 1 mol/L NaI is negligible (<4%) when compared with those of a flat interface where the average emission angle is taken to be 0° . We predict that such a small difference in ion intensity ratio could not be determined by experiment. We therefore conclude that XPS results from the two different sample configurations, assumed flat in the case of deliquesced salt crystals and cylindrical in the case of the microjet, are essentially the same and can be compared without having to worry about the influence of the microjet's curvature.

Acknowledgements

G.O. is funded through at ETH Research Grant (no. ETH-20 13-2). The work at UC Irvine is supported in part by a grant from the National Science Foundation (no. CHE-0431312).

Notes and references

- H. Siegbahn and K. Siegbahn, *Journal of Electron Spectroscopy and Related Phenomena*, 1973, 2, 319-325.
- B. Winter and M. Faubel, *Chem Rev*, 2006, 106, 1176-1211.
- M. A. Brown, M. Faubel and B. Winter, *Annual Reports on the Progress of Chemistry, Section C*, 2009, 105, 174-212.
- M. A. Brown, I. Jordan, A. Beloqui Redondo, A. Kleibert, H. J. Wörner and J. A. van Bokhoven, *Surf Sci*, 2013, 610, 1-6.
- G. Olivieri, K. M. Parry, C. J. Powell, D. J. Tobias and M. A. Brown, *J Chem Phys*, 2016, 144, 154704.
- S. Ghosal, J. C. Hemminger, H. Bluhm, B. S. Mun, E. L. D. Hebenstreit, G. Ketteler, D. F. Ogletree, F. G. Requejo and M. Salmeron, *Science*, 2005, 307, 563-566.
- M. J. Krisch, R. D'Auria, M. A. Brown, D. J. Tobias, J. C. Hemminger, M. Ammann, D. E. Starr and H. Bluhm, *J Phys Chem C*, 2007, 111, 13497-13509.
- M. A. Brown, R. D'Auria, I. F. W. Kuo, M. J. Krisch, D. E. Starr, H. Bluhm, D. J. Tobias and J. C. Hemminger, *Phys Chem Chem Phys*, 2008, 10, 4778-4784.
- M. A. Brown, B. Winter, M. Faubel and J. C. Hemminger, *Journal of the American Chemical Society*, 2009, 131, 8354-8355.
- N. Ottosson, R. Vacha, E. F. Aziz, W. Pokapanich, W. Eberhardt, S. Svensson, G. Ohrwall, P. Jungwirth, O. Bjorneholm and B. Winter, *J Chem Phys*, 2009, 131, 124706.
- M. H. Cheng, K. M. Callahan, A. M. Margarella, D. J. Tobias, J. C. Hemminger, H. Bluhm and M. J. Krisch, *J Phys Chem C*, 2012, 116, 4545-4555.
- H. Tissot, G. Oivieri, J. J. Gallet, F. Bournel, M. G. Silly, F. Sirotti and F. Rochet, *J Phys Chem C*, 2015, 119, 9253-9259.
- M. A. Brown, M. T. Lee, A. Kleibert, M. Ammann and J. B. Giorgi, *J Phys Chem C*, 2015, 119, 4976-4982.
- C. J. Powell and A. Jablonski, *Nucl Instrum Meth A*, 2009, 601, 54-65.
- A. Jablonski and C. J. Powell, *J. Vac. Sci. Technol. A*, 2009, 27, 253.
- W. Smekal, W. S. M. Werner and C. J. Powell, *Surf Interface Anal*, 2005, 37, 1059-1067.
- W. S. M. Werner, W. Smekal and C. J. Powell, *NIST Database for the Simulation of Electron Spectra for Surface Analysis, Version 2.0, Standard Reference Data Program Database 100, Department of Commerce, National Institute of Standards and Technology*, Gaithersburg, Maryland, 2014.
- S. Tanuma, C. J. Powell and D. R. Penn, *Surf Interface Anal*, 1994, 21, 165-176.
- Y. I. Suzuki, K. Nishizawa, N. Kurahashi and T. Suzuki, *Phys Rev E*, 2014, 90, 010302.
- http://www.specs.de/cms/front_content.php?idcat=269, Accessed June 23, 2016.
- S. Techane, D. R. Baer and D. G. Castner, *Anal Chem*, 2011, 83, 6704-6712.
- W. S. M. Werner, I. S. Tilinin and A. Jablonski, *Surf Interface Anal*, 1995, 23, 823-832.
- Larger ϕ are in principle possible with magnetic-bottle flight-tube analysers,²⁷ but in practice the small entrance aperture needed for ambient pressure and liquid jet type experiments limits ϕ to values much smaller than those achieved with commercial hemispherical analysers.²⁸ In addition, magnetic-bottle flight-tube analysers are operated at synchrotron radiation facilities typically only when the storage ring is operated in a single- or two-bunch mode. Depth-resolved energy-dependent XPS experiments have, to-date, only been done in multi-bunch mode, which make these analysers ill-suited for the type of experiment considered herein.
- D. J. Tobias, A. C. Stern, M. D. Baer, Y. Levin and C. J. Mundy, *Annu Rev Phys Chem*, 2013, 64, 339-359.
- A. P. Willard and D. Chandler, *J Phys Chem B*, 2010, 114, 1954-1958.
- The SESSA intensities for I 4d and Na 2p are normalized by the corresponding energy-dependent photoionization cross-sections. In Fig. ESI-3 we show that the cross-sections employed herein yield stoichiometric ion ratios for a homogeneous solution of 1 mol/L NaI for all kinetic energies.
- T. Tsuboi, E. Y. Xu, Y. K. Bae, K. T. Gillen, *Rev Scient Instr*, 1988, 59, 1357-1362.
- A. Kothe, J. Metje, M. Wilke, A. Moguelevski, N. Engel, R. Al-Obaidi, C. Richter, R. Golnak, I. Yu. Kiyani, E. F. Aziz, *Rev Sci Instrum*, 2013, 84, 0231



Journal Name

COMMUNICATION



Journal Name

COMMUNICATION

Electronic Supplementary Information (ESI) for:

Simulated photoelectron intensities at the aqueous solution–air interface for flat and cylindrical (microjet) geometries

Giorgia Olivieri,^a Krista M. Parry,^b Cedric J. Powell,^c Douglas J. Tobias,^b and Matthew A. Brown^{a*}

^aLaboratory for Surface Science and Technology, Department of Materials, ETH Zürich, Switzerland.

^bDepartment of Chemistry, University of California, Irvine, California, USA.

^cMaterials Measurement Science Division, National Institute of Standards and Technology, Gaithersburg, Maryland, USA.

E-mail: matthew.brown@mat.ethz.ch

Table ESI-1. Information depths ($P = 95\%$, $\alpha = 0^\circ$) for semi-infinite bulk solutions of pure water and homogeneous 1 mol/L NaI calculated using SESSA with linear polarized light. Information depths extrapolated from a linear fit of the calculated values are marked with an asterisk.

Kinetic Energy (eV)	S (nm)	
	H ₂ O	1 mol/L NaI
65	1.47	1.40
100*	1.97	1.89
150*	2.37	2.27
200	2.71	2.60
250*	3.17	3.04
300*	3.57	3.42
350*	3.97	3.80
400*	4.37	4.18
450*	4.78	4.57
500	5.36	5.13
550*	5.58	5.33
600*	5.98	5.71
650*	6.38	6.09
700*	6.78	6.48
750*	7.18	6.86
800	7.88	7.53
850*	7.98	7.62
900*	8.38	8.01
950*	8.78	8.39
1000	9.22	8.81
1050*	9.58	9.15
1100*	9.98	9.53
1150*	10.38	9.92
1200*	10.78	10.30
1250	11.12	10.63
1300*	11.58	11.06
1350*	11.98	11.45
1400*	12.38	11.83
1450*	12.78	12.21
1500	13.00	12.41

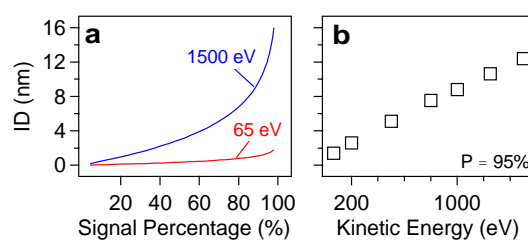


Fig. ESI-1. (a) Information depth (ID) at 65 eV and 1500 eV of a semi-infinite solution of 1 mol/L NaI as a function of the percentage of the detected signal when using linear polarized light and $\alpha = 0^\circ$. (b) IDs of liquid water for $P=95\%$ as a function of photoelectron kinetic energy when $\alpha = 0^\circ$.

Methods

Simulation of Electron Spectra for Surface Analysis (SESSA). XPS signal intensities are simulated using the SESSA software package developed by Werner *et al.*¹ SESSA is a NIST standard reference database² that contains all data needed for quantitative simulations of XPS and Auger-electron spectra. Data retrieval is based on an expert system that queries the databases for each needed parameter. SESSA provides the spectral shape of each photoelectron peak using a model of signal generation in XPS that includes multiple inelastic and elastic scattering of the photoelectrons. In order to minimize the computation time, an efficient

Monte Carlo code is employed based on the trajectory-reversal method. In contrast to conventional Monte Carlo codes where electrons are tracked based on their trajectories from the source to the detector, the trajectory-reversal approach tracks electrons in the opposite direction, starting from the detector and working back to the point of origin. Thus, all electrons contribute to the signal, which results in significantly decreased simulation times.

For the SESSA simulations reported in this Communication, the orientation of the analyzer axis is perpendicular to the X-ray source, while the sample surface normal orientation is varied from 0° (parallel to the analyzer axis) to 90° (perpendicular to the analyzer axis). The excitation source is a linearly polarized X-ray beam. The polarization vector is rotated 54.7° from the analyzer detection axis, which corresponds to the so-called magic angle in which the XPS intensity is independent of the emission angle. Since we are simulating synchrotron-based experiments in which X-rays are focused in a relatively small area, the illuminated area on the sample is independent of the emission angle.

Other details of our SESSA simulations have been discussed previously.³ A convergence factor of 10^{-6} has been used for all simulations and the Mott approximation has been used to take into account elastic-scattering effects. The total density for pure water and bulk 1 mol/L NaI has been set to 9.90×10^{22} atoms/cm³ and 9.42×10^{22} atoms/cm³, respectively, while the band gap is assumed 7.9 eV for both solutions. Our calculations employ electron IMFPs calculated via the semi-empirical TPP-2M formula of Tanuma *et al.*⁴ integrated within SESSA. The calculated IMFPs, which depend on the material density, atomic or molecular mass, number of valence electrons per atom or molecule, and the band gap energy, are expected to have uncertainties of about 10%, although the uncertainty could be larger for a small number of materials. For the Na/I ion intensity ratios a total of 13 photoelectron energies were simulated and the simulated intensities were normalized by the atomic photoionization cross sections of Yeh and Lindau⁵ integrated within SESSA.

Molecular Dynamics (MD) Simulations. Molecular dynamics simulations of the 1 mol/L NaI solution were performed using the GROMACS simulation suite³. 1728 water molecules and 32 NaI ion pairs were placed in a 3.0 nm x 3.0 nm x 14.0 nm unit cell in the slab geometry. Periodic boundary conditions were implemented in all three dimensions. The simulation was carried out for 100 μ s using a timestep of 2 fs. The temperature was held at 300 K using a Berendsen thermostat with an additional stochastic term that ensures the correct kinetic energy distribution.⁴ Water molecules were modeled using the Simple Point Charge/Extended (SPC/E) force field,⁵ and the Lennard-Jones parameters for the ions were parameterized by Netz and coworkers.⁶ Electrostatic interactions were calculated using the Particle-Mesh Ewald method,⁷ and a cutoff of 0.9 nm was used for the Lennard-Jones interactions and the real-space part of the Ewald sum. Water molecules were held rigid using the SETTLE algorithm.⁸ Atom density profiles were computed with respect to the instantaneous interface as described previously.^{9,10} The average bulk concentration calculated from the composition of the innermost 2 nm of the slab was 0.96 mol/L.

Liquid jet properties. Not all readers are familiar with the liquid jets used for XPS experiments. Here we provide a few key details that might help to better understand the simulation results of the main manuscript. Liquid jets are generated by forcing the liquid under investigation through thin quartz capillaries of inner diameter \sim 6–30 μ m using a standard commercial high-pressure liquid chromatography (HPLC) pump. These liquid jets are free flowing inside the vacuum chamber and provide a continuously refreshed interface. The liquid jet is spatially overlapped with synchrotron radiation and XPS is performed. The typically size of the X-ray beam (fwhm) is on the order of 10's of μ m.

Calculation of the information depth (ID)

The IDs of Table ESI-1 are calculated for semi-infinite solutions using SESSA. For this purpose the sample has been sliced into layers and the photoelectron intensity of the O 1s has been simulated for each layer separately for a given photoelectron kinetic energy. By doing this operation the total photoelectron signal is obtained as a function of depth and it is then easy to convert it into an ID as a function of the signal percentage. The number of slices as well as the slices' thickness varied with the kinetic energy of the photoelectron in order to adjust the total sample thickness to the ID for that particular energy. All the simulations have been performed with linearly polarized light at the so-called magic angle. The analyser polar acceptance angle is 1° and the average emission angle of the photoelectrons is 0°.

Average emission angle of a cylindrical microjet of pure water

In order to calculate the limit in Eq. 2 of the main text we have simulated the O 1s intensity for a microjet of pure water using SESSA for 91 surface tilt angles between 0° and 90° in increments of 1°. The average emission angle is calculated (see Fig. ESI-2) using planes with separation of 1°, 2°, 5° or 10°, which corresponds to using 91, 46, 19 and 10 planes, respectively. As the number of planes tends to infinity the surface tilt angle increments tend to zero. For this reason, an extrapolation of the average emission angle to zero surface tilt angle step is necessary to find the correct average emission angle. The results of Fig. ESI-2 show a linear extrapolation.

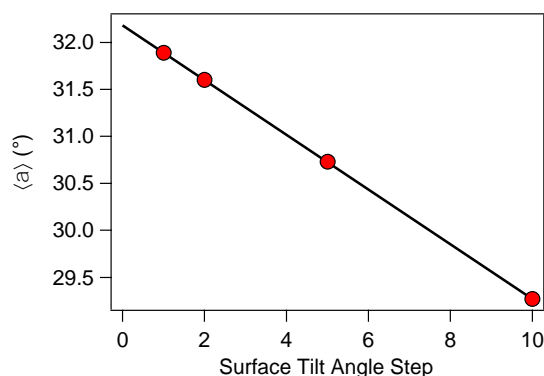


Fig. ESI-2. Average emission angle as a function of the surface tilt angle increment. A linear extrapolation to $x = 0$ yields the average emission angle used in the main text.

Comparison of the average emission angle of a cylindrical microjet of pure water with that of a homogeneous solution of 1 mol/L NaI

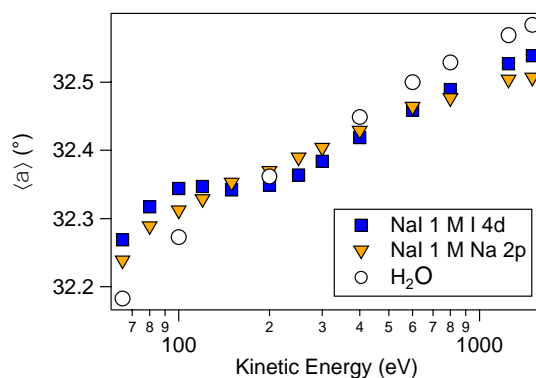


Fig. ESI-3. Average emission angle for a cylindrical microjet of pure water (open black markers) and for a homogeneous solution of 1 mol/L NaI.

I 4d/Na 2p ratio for a homogeneous solution of 1 mol/L NaI as a function of kinetic energy

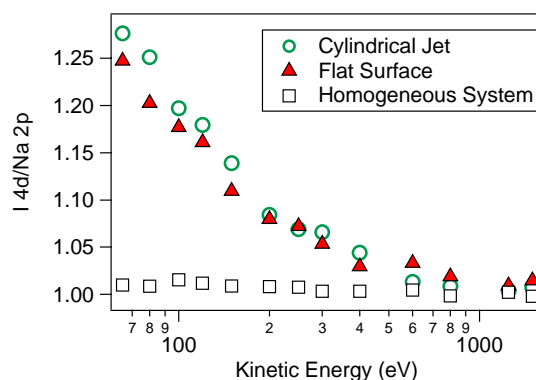


Fig. ESI-4. (open black squares) I 4d/Na 2p ion ratios calculated from SESSA simulation for a semi-infinite bulk homogeneous solution of 1 mol/L NaI. These results verify that the cross-sections used to normalize the simulated photoelectron intensities result in stoichiometric ion intensity ratios for all kinetic energies. Results for the complete molecular dynamics interface are included for comparison (these data are plotted in Fig. 4 of the main text).

References

1. W. Smekal, W. S. M. Werner and C. J. Powell, *Surf Interface Anal*, 2005, 37, 1059-1067.
2. W. S. M. Werner, W. Smekal and C. J. Powell, *NIST Database for the Simulation of Electron Spectra for Surface Analysis, Version 2.0, Standard Reference Data program Database 100*, Department of Commerce, National Institute of Standards and Technology, Gaithersburg, Maryland, 2014.
3. G. Olivieri, K. M. Parry, C. J. Powell, D. J. Tobias, and M. A. Brown, *J Chem Phys.*, 2016, **144**, 154704.
4. S. Tanuma, C. J. Powell, and D. R. Penn, *Surf. Interface Anal.*, 1994, 21, 165-176.
5. J. J. Yeh and I Lindau, *Atom Data Nucl Data*, **1985**, 32, 1-155.
6. B. Hess, C. Kutzner, D. van der Spoel and E. Lindahl, *J Chem Theory Comput*, 2008, 4, 435-447.
7. G. Bussi, D. Donadio and M. Parrinello, *J Chem Phys*, 2007, 126.
8. H. J. Berendsen, J. R. Grigera and T. P. Straatsma, *J Phys Chem-Us*, 1987, 91, 6269-6271.
9. D. Horinek, A. Herz, L. Vrbka, F. Sedlmeier, S. I. Mamatkulov and R. R. Netz, *Chem Phys Lett*, 2009, 479, 173-183.
10. U. Essmann, L. Perera, M. L. Berkowitz, T. Darden, H. Lee and L. G. Pedersen, *J Chem Phys*, 1995, 103, 8577-8593.
11. S. Miyamoto and P. A. Kollman, *J Comput Chem*, 1992, 13, 952-962.
12. A. P. Willard and D. Chandler, *J Phys Chem B*, 2010, 114, 1954-1958.